

# Correcting for fibre assignment incompleteness in the DESI Bright Galaxy Survey

Alex Smith,<sup>1,2★</sup> Jian-hua He,<sup>2</sup> Shaun Cole,<sup>2</sup> Lee Stothert,<sup>2,3</sup> Peder Norberg,<sup>2,3</sup> Carlton Baugh,<sup>2</sup> Davide Bianchi,<sup>4</sup> Michael J. Wilson,<sup>5</sup> David Brooks,<sup>6</sup> Jaime E. Forero-Romero,<sup>7</sup> John Moustakas,<sup>8</sup> Will J. Percival,<sup>4,9,10</sup> Gregory Tarle<sup>11</sup> and Risa H. Wechsler<sup>12,13</sup>

<sup>1</sup>IRFU, CEA, Université Paris-Saclay, F-91191 Gif-sur-Yvette, France

<sup>2</sup>Institute for Computational Cosmology, Department of Physics, University of Durham, South Road, Durham DH1 3LE, UK

<sup>3</sup>Centre for Extragalactic Astronomy, Department of Physics, University of Durham, South Road, Durham DH1 3LE, UK

<sup>4</sup>Institute of Cosmology & Gravitation, University of Portsmouth, Dennis Sciama Building, Portsmouth PO1 3FX, UK

<sup>5</sup>Lawrence Berkeley National Laboratory, 1 Cyclotron Road, Berkeley, CA 94720, USA

<sup>6</sup>Department of Physics & Astronomy, University College London, Gower Street, London WC1E 6BT, UK

<sup>7</sup>Departamento de Física, Universidad de los Andes, Cra. 1 No. 18A-10, Edificio Ip, CP 111711, Bogotá, Colombia

<sup>8</sup>Department of Physics and Astronomy, Siena College, 515 Loudon Road, Loudonville, NY 12211, USA

<sup>9</sup>Department of Physics and Astronomy, University of Waterloo, 200 University Ave. W, Waterloo, ON N2L 3G1, Canada

<sup>10</sup>Perimeter Institute for Theoretical Physics, 31 Caroline Str North, Waterloo, ON N2L 2Y5, Canada

<sup>11</sup>Physics Department, University of Michigan Ann Arbor, MI 48109, USA

<sup>12</sup>Kavli Institute for Particle Astrophysics and Cosmology and SLAC National Accelerator Laboratory, Menlo Park, CA 94305, USA

<sup>13</sup>Physics Department, Stanford University, Stanford, CA 93405, USA

Accepted 2018 December 21. Received 2018 November 28; in original form 2018 September 19

## ABSTRACT

The Dark Energy Spectroscopic Instrument (DESI) Bright Galaxy Survey (BGS) will be a survey of bright, low-redshift galaxies, which is planned to cover an area of  $\sim 14\,000$  square degrees in three passes. Each pass will cover the survey area with  $\sim 2000$  pointings, each of area  $\sim 8$  square degrees. The BGS is currently proposed to consist of a bright high priority sample to an  $r$ -band magnitude limit  $r \sim 19.5$ , with a fainter low priority sample to  $r \sim 20$ . The geometry of the DESI fibre positioners in the focal plane of the telescope affects the completeness of the survey and has a non-trivial impact on clustering measurements. Using a BGS mock catalogue, we show that completeness due to fibre assignment primarily depends on the surface density of galaxies. Completeness is high ( $>95$  per cent) in low-density regions, but very low ( $<10$  per cent) in the centre of massive clusters. We apply the pair inverse probability (PIP) weighting correction to clustering measurements from a BGS mock which has been through the fibre assignment algorithm. This method is only unbiased if it is possible to observe every galaxy pair. To facilitate this, we randomly promote a small fraction of the fainter sample to be high priority, and dither the set of tile positions by a small angle. We show that inverse pair weighting combined with angular upweighting provides an unbiased correction to galaxy clustering measurements for the complete three pass survey, and also after one pass, which is highly incomplete.

**Key words:** galaxies: statistics – cosmology: observations – (cosmology:) large-scale structure of Universe.

## 1 INTRODUCTION

The Dark Energy Spectroscopic Instrument (DESI; DESI Collaboration et al. 2016a,b) will conduct a large spectroscopic survey with the primary science aims of making precision measurements of the baryon acoustic oscillation (BAO) scale and the large-scale

\* E-mail: alexander.smith@cea.fr

redshift space distortion (RSD) of galaxy clustering. BAO will be used to measure the expansion history of the Universe and constrain dark energy (e.g. Seo & Eisenstein 2003). RSD will be used to measure the growth rate of structure in the Universe, and place constraints on theories of modified gravity (e.g. Guzzo et al. 2008). These measurements are complementary, as they can be used to break degeneracies between models of dark energy and RSD. The instrument, which is nearing completion, will be installed on the 4-m Mayall Telescope at Kitt Peak, Arizona. DESI will consist of dark-time and bright-time programmes. The dark-time survey will measure spectra of 4 million luminous red galaxies (LRGs) ( $0.4 < z < 1.0$ ), 17 million emission line galaxies (ELGs) ( $0.6 < z < 1.6$ ), 1.7 million quasars ( $z < 2.1$ ), and 0.7 million high-redshift quasars ( $2.1 < z < 3.5$ ) to probe the Ly  $\alpha$  forest. The bright-time survey will consist of the Bright Galaxy Survey (BGS), a low-redshift, flux-limited survey of  $\sim 10$  million galaxies with a median redshift  $z_{\text{med}} \sim 0.2$  (BGS paper, in preparation), and a survey of Milky Way stars (DESI Collaboration et al. 2016a).

The light from each target galaxy is collected by fibres located at the focal plane of the telescope, and taken to one of 10 spectrographs, where the spectrum is measured and a redshift determined. However, it is not possible to place a fibre on every single potential target, and even if it is, a redshift measurement can fail due to low surface brightness or weak spectral features. Other complications, such as observing conditions, also affect the redshift completeness in the final galaxy catalogue.<sup>1</sup> To make precise measurements of galaxy clustering in order to reach the primary science aims of the survey, it is essential to correct for the effects of incompleteness.

A major systematic in galaxy clustering measurements is from the effect of fibre collisions, which occur because fibres cannot be placed arbitrarily close together. Since it is not possible to place a fibre on both objects in a close pair, that pair will be missing in the final catalogue, biasing the pair counts, particularly at small scales, which can bias galaxy clustering measurements. If the same patch of sky is observed enough times, the missing galaxies will eventually be observed, removing the bias (e.g. in GAMA Robotham et al. 2010), but typically it is infeasible to do this.

In the Sloan Digital Sky Survey (SDSS; Abazajian et al. 2009), the fibre collisions can be characterized relatively straightforwardly, since fibres can be placed anywhere on a plate, so long as they are not closer than the fibre collision scale of 55 arcsec (or 62 arcsec for BOSS). A common method to recover the redshift of missing galaxies is to simply assign them the same redshift as the nearest targeted object on the sky (e.g. Zehavi et al. 2005, 2011). However, this method produces unsatisfactory results for the redshift–space correlation function (as shown in Section 4.3.2). An alternative method that works well for SDSS involves recovering the full correlation function from the regions covered by multiple overlapping tiles (Guo, Zehavi & Zheng 2012). In dense regions, SDSS is able to target all galaxies, or an unbiased subset, but this is not true for the BGS.

Fibre collisions in DESI are more complicated, since the fibres are controlled by robotic fibre positioners, which can move each fibre anywhere in a small patrol region around a fixed set of centres, arranged in a grid. The fibre positioners can block neighbouring fibres from targeting certain objects, and objects will be missed if the number density of targets in an extended region is greater than the number density of fibres. These effects have a non-trivial

<sup>1</sup>Exposures are scaled dynamically with conditions, with the aim of achieving a consistent signal-to-noise ratio in the spectra.

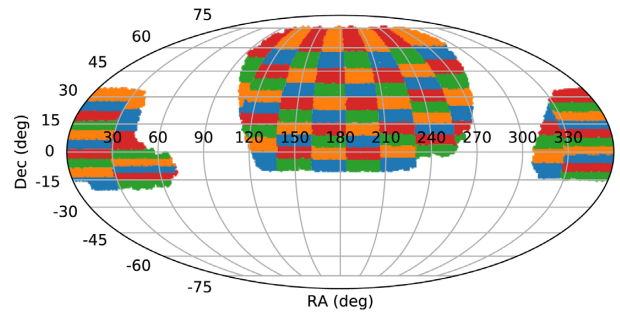


**Figure 1.** Footprint of the DESI BGS, which covers 14 800 square degrees. Colours indicate the 100 jackknife regions.

impact on clustering estimates. The statistics to be measured from the survey can be modified to remove the affected scales (e.g. Burden et al. 2017; Pinol et al. 2017), but in doing so, information is lost. Bianchi & Percival (2017) have proposed a method to correct clustering measurements by estimating, from many runs of the fibre assignment algorithm, the probability that a pair of galaxies will be targeted, and have shown that this method can provide an unbiased correction to the dark-time ELG sample (Bianchi et al. 2018). The method has also been shown to be successful when applied to data from the VIPERS survey (Mohammad et al. 2018).

Galaxies in the BGS have a variety of properties, and cover a wide range of galaxy bias. Many kinds of galaxy samples can be selected from the survey, such as volume limited samples, stellar-mass selected samples and colour-selected samples. Here, we quantify the incompleteness due to fibre assignment in the DESI BGS, and assess correlation function correction techniques applied to samples from a BGS mock catalogue. This paper is organized as follows. In Section 2, we describe the BGS survey strategy, DESI fibre assignment, and mock survey simulations. In Section 3, we quantify galaxy incompleteness in the BGS due to fibre assignment. In Section 4, we assess correlation function correction methods on volume-limited samples from the BGS mock. Section 5 summarizes our conclusions. Throughout, we assume the WMAP-1 cosmology of the mock catalogue presented in Section 2.4, with  $\Omega_m = 0.25$ ,  $\Omega_\Lambda = 0.75$ ,  $\sigma_8 = 0.9$ ,  $h = 0.73$ , and  $n = 1$  (Spergel et al. 2003). While this cosmology has a higher  $\sigma_8$  and lower  $\Omega_m$  than measurements from Planck (Planck Collaboration VI, 2018), we use simulations tuned to produce the correct galaxy clustering, so we expect the dependence of our results on cosmology to be small.

## 2 FIBRE ASSIGNMENT

### 2.1 Survey strategy

The aim of the DESI BGS is to create a highly complete flux-limited catalogue of bright, low-redshift galaxies, for the primary science goals of BAO and RSD analysis. The survey is expected to cover  $\sim 14\,000$  square degrees (Fig. 1) in three passes of the sky, measuring spectroscopic redshifts of  $\sim 10$  million galaxies, approximately 2 mag deeper than the SDSS main survey (Strauss et al. 2002), with double the median redshift ( $z_{\text{med}} \sim 0.2$ ). The BGS will take place concurrently with the Milky Way Survey during bright time, when the sky is too bright for the main dark-time survey due to moon phase and twilight conditions.

Fibres are currently planned to be assigned to science targets based on the following priority tiers:

- (i) Priority 1 galaxies ( $r < r_{\text{bright}}$ ,  $\sim 800 \text{ deg}^{-2}$ )

**Table 1.** Percentage of the survey area covered by  $N$  overlapping tiles after 1 pass with 10 per cent of tiles missing, and after the full one, two, and three passes. The total area covered by each pass is calculated by finding the fraction of objects in a random catalogue that can be potentially assigned a fibre.

$N$	Pass 1 (90 per cent)	Pass 1	Pass 2	Pass 3
	(12.2k deg <sup>2</sup> )	(13.5k deg <sup>2</sup> )	(14.6k deg <sup>2</sup> )	(14.8k deg <sup>2</sup> )
1	89.8	88.4	13.4	3.6
2	10.2	11.6	67.3	14.9
3	0.01	0.01	18.4	55.9
4	0.0	0.0	0.9	23.1
5	0.0	0.0	0.009	2.3
6	0.0	0.0	0.0	0.1
7	0.0	0.0	0.0	0.006

- (ii) Priority 2 galaxies ( $r_{\text{bright}} < r < r_{\text{faint}}$ ,  $\sim 600 \text{ deg}^{-2}$ )
- (iii) Milky Way stars

Here,  $r_{\text{bright}} \sim 19.5$  and  $r_{\text{faint}} \sim 20.0$ <sup>2</sup>

The brightest galaxies with an  $r$ -band magnitude  $r < 19.5$  are preferentially targeted, since the redshift success rate is expected to be high, making this sample of galaxies highly complete. Fainter galaxies, with  $19.5 < r < 20.0$ , which have a lower redshift success rate, are given a lower priority, and will form a less complete sample. If a fibre cannot be placed on a galaxy, it will be placed on a Milky Way star.

If a galaxy fails to have its redshift measured, one possibility is for it to remain at the same priority in the next pass. If a redshift is successfully measured, it will remain a potential target in future passes to give the possibility of improving the signal-to-noise ratio of the spectra, but its priority demoted to a fourth priority tier (below that of the Milky Way stars).

In addition to the galaxy targets, 100 fibres will be positioned on standard stars and 400 on blank sky locations (sky fibres) in each exposure, with an equal number per petal (see Section 2.2), for flux calibration and sky subtraction.

The observation strategy that will be used in the BGS is still to be chosen. We assume a strategy in which the three complete passes of the entire survey are observed sequentially. Each pass consists of  $\sim 2000$  tiles positioned over the entire survey footprint, with overlaps between neighbouring tiles. In the first pass, the tile centres are positioned on the sky with an icosahedral tiling. The tiling for subsequent passes is identical, except with a rotation on the sky, which fills in the missing area due to gaps in the focal plane. The percentage of the survey footprint that is covered by  $N$  overlapping tiles after each full pass, and also after 90 per cent of the first pass,<sup>3</sup> is summarized in Table 1. After 1 pass,  $\sim 90$  per cent of the footprint is covered by a single tile. This is greatly reduced after subsequent passes, with  $\sim 80$  per cent covered by three or more tiles at the end of the survey. These numbers take into account the gaps in the focal plane.

<sup>2</sup>In Section 2.4, we use  $r_{\text{bright}} = 19.452$  and  $r_{\text{faint}} = 19.925$ , which in the BGS mock catalogue gives number densities of  $818 \text{ deg}^{-2}$  and  $618 \text{ deg}^{-2}$  for the bright and faint samples, respectively. We also randomly promote 10 per cent of the faint sample to have the same priority as the bright sample (see Section 2).

<sup>3</sup>90 per cent of one pass is chosen as a realistically incomplete dataset, representing what might be available one third of the way through the survey, where certain fields are missed due to observing conditions.

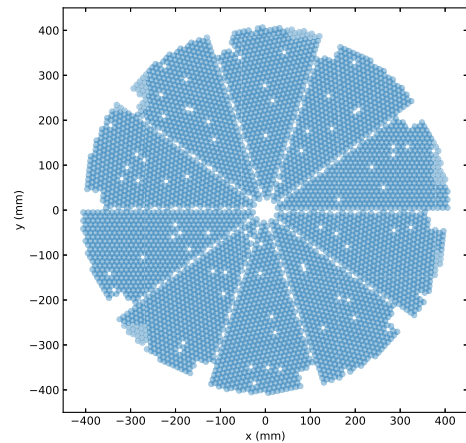


**Figure 2.** A single DESI tile, showing the arrangement of fibres in the focal plane, split into 10 petals. The blue circles indicate the patrol area of each fibre. The holes within each petal are the locations of the fiducials, which provide a light source for the fibre view camera to calibrate the placement of the fibre positioners.

## 2.2 Robotic fibre positioners

Each pointing of DESI, or tile, consists of a total of 5000 fibres, arranged on the focal plane in 10 wedge-shaped ‘petals’ (Schubnell et al. 2016). Each individual fibre is controlled by a robotic fibre positioner that can rotate on two arms, allowing the fibre to be placed on any object within a unique circular patrol region (see e.g. fig. 3.11 of DESI Collaboration et al. 2016b), with a patrol radius corresponding to an angle on the sky of  $R_{\text{patrol}} = 1.48 \text{ arcmin}$  ( $0.0247 \text{ deg}$ ) (at  $z = 0.2$ , this is a comoving separation of  $0.25 h^{-1} \text{ Mpc}$ ). The arrangement of fibres is illustrated in Fig. 2. There is a small overlap between the patrol regions of neighbouring fibres, and there are gaps between petals that cannot be reached by a fibre. The ‘missing’ squares around the edge of the tile are the location of the guide focus arrays, which measure the pointing of the telescope and orientation of the focal surface. Each petal also contains 10 fiducials that provide light sources for the fibre view camera to calibrate fibre positioner placement (section 3.5 of DESI Collaboration et al. 2016b).

## 2.3 Fibre assignment algorithm

To assign fibres to targets, each potential target object is first assigned a primary priority, which is an integer that is determined by the priority tier of the object, e.g. all priority 1 galaxies have the same primary priority, which is numerically greater than the priority 2 galaxies. A uniform random sub-priority in the range (0,1) is then generated for each object, and the total priority is the sum of the primary and sub-priorities. Fibres are ordered by the highest priority object in their patrol region (from highest to lowest numerical value), and are looped through in this order. Each fibre in turn is assigned to the object in its patrol region with the highest priority it is possible for it to target. With this scheme, the assignment of fibres to objects in the same priority tier is randomized, but if a high-priority object competes for a fibre with a low-priority object, the high-priority object will always be assigned a fibre at the expense of the low-priority object. If fibres are instead looped through in a fixed order, certain fibres would always have a high priority, and be assigned to a galaxy before its six neighbouring fibres, potentially

preventing them from ever targeting certain objects due to fibre collisions.

In the current survey strategy, the entire survey is split into several epochs. In each epoch, tiles are selected by a survey planning algorithm, which determines the sequence of tiles based on date and survey conditions. The selected tiles then go through the fibre assignment algorithm. The fibre assignment algorithm loops through each tile, in a fixed order, assigning fibres to objects. At the end of this loop, there is some redistribution of fibres so that

- (i) the total number of targets observed is maximized,
- (ii) there are the required number of standard stars and sky fibres,
- (iii) fibres that are unused are uniformly distributed over tiles.

After fibre assignment, at the end of the epoch, galaxy priorities are updated depending on whether the redshift measurement was successful or unsuccessful. The updated galaxy priorities are then used in the next epoch.

In order to make unbiased 2-point galaxy clustering measurements using the Bianchi & Percival (2017) scheme, each pair of objects in the parent sample must have a non-zero probability of being targeted (see Section 4.1.3). To make sure as many pairs as possible can be targeted, we do the following.

### 2.3.1 Dithering tile positions

In regions covered by a single tile, if there are two priority 1 galaxies in the unique patrol region of a single fibre, that fibre will target the galaxy with the numerically highest random sub-priority, but it can never target both, so the pair will always be missed.

This can be mitigated by, in each realization of fibre assignment, applying a global dither to the tiling of the entire survey, i.e. randomly rotating the whole three-pass set of survey tiles by a small angle (of the order of  $R_{\text{patrol}}$ ). This is entirely equivalent to keeping the tiling fixed in each realization, and rotating the galaxy positions on the celestial sphere. In some of these random dithers, the two objects in an untargetable pair will be split between two neighbouring fibres, giving the pair a non-zero probability of being targeted. Since tile centres are uncorrelated with large-scale structure, galaxy pairs of any separation in any environment are equally likely to be targeted in each realization, and therefore it is valid to average over realizations to estimate the probability. To dither the tile positions, a random rotation axis is chosen, which is uniformly distributed. The tile centres are then rotated around this axis by a small angle, which we choose to be three times the fibre patrol radius.

The dithering of the tile positions is only done when applying the pair weighting correction described in Section 4.1.3. When assigning fibres to objects in the real survey, the rotation angle is set to zero.

### 2.3.2 Priority 2 galaxies

Priority 1 galaxies always have a higher priority than priority 2 galaxies, so if it is possible for a fibre to be placed on an unobserved priority 1 galaxy, it will always target that galaxy, regardless of how many priority 2 galaxies are in the same patrol region. This means that a significant fraction of priority 2 galaxies in regions with a high density of priority 1 galaxies will always be missed.

One way of sampling these missing priority 2 galaxies is, in each fibre assignment realization, to randomly promote a certain fraction of priority 2 galaxies to the same priority as the priority 1

galaxies. This gives pairs containing at least one priority 2 galaxy in overdense regions a small, but non-zero probability of being targeted (see Fig. 3).

The version of the fibre assignment algorithm we use is 0.6.0.<sup>4</sup>

## 2.4 Survey simulations

To quantify incompleteness due to fibre assignment and assess correlation function correction methods, we run the fibre assignment algorithm on a BGS mock catalogue from the Millennium-XXL (MXXL) simulation (Smith et al. 2017). This is a halo occupation distribution (HOD) mock, which contains galaxies to  $r = 20$  over the same redshift range as the BGS, and is constructed to reproduce the luminosity function and clustering measurements from SDSS (Blanton et al. 2003; Zehavi et al. 2011) and GAMA (Loveday et al. 2012; Farrow et al. 2015).<sup>5</sup>

The magnitudes in this catalogue are in the SDSS  $r$ -band. These are converted to the DECam  $r$ -band (which is used in the DESI target selection) using

$$r_{\text{DECam}} = r_{\text{SDSS}} - 0.03587 - 0.14144(r - i)_{\text{SDSS}}. \quad (1)$$

Since the mock catalogue does not contain  $r - i$  colours, we assume a mean colour of  $(r - i) = 0.4$ . To make sure the priority 1 and 2 galaxies have number densities of  $818 \text{ deg}^{-2}$  and  $618 \text{ deg}^{-2}$ , we define priority 1 and 2 galaxies using the magnitudes  $r_{\text{DECam}} = 19.452$  and  $r_{\text{DECam}} = 19.925$ .<sup>6</sup>

The mock is first cut to the set of galaxies that are within the patrol radius of a fibre in the full three-pass survey (with no dither), and therefore could potentially be assigned a fibre.<sup>7</sup> We run 2048 random realizations of the fibre assignment algorithm ( $\sim 500$  CPU hours), with the full three passes of tiles to simulate the complete survey. From the survey simulation output, it is also possible to determine which galaxies were assigned fibres in the first or second pass, allowing us to simulate a more incomplete survey without having to re-run the fibre assignment code. In addition to the full three passes, we also determine which galaxies are targeted in one pass, with a random 10 per cent of tiles missing (which are the same tiles in each realization), to simulate a data set that might realistically be achieved after one-third of the duration of the survey with a survey strategy that prioritizes area (i.e. a strategy where after one-third of the duration, pass 1 is completed, as opposed to a strategy where three passes are completed in only one-third of the survey area). Removing tiles reduces the overall area of the footprint and increases the fraction of the remaining area that is covered by a single tile.

In each run of the fibre assignment code, the tile positions are randomly dithered by an angle three times the patrol radius, and a random 10 per cent of priority 2 galaxies are promoted to the same priority as the bright sub-sample. Unless specified, we will refer to the bright sub-sample as ‘priority 1’ and the faint sub-sample as ‘priority 2’.

<sup>4</sup><https://github.com/desihub/desitarget>

<sup>5</sup>The MXXL mock is available at <http://icc.dur.ac.uk/data/> and <https://tao.asvo.org.au/tao/>

<sup>6</sup>These number densities are chosen to match assumptions made in earlier survey simulations (Tinker, private communication).

<sup>7</sup>In our clustering analysis, we account for the regions of sky this process discards by applying the same criterion to the corresponding random catalogue. This differs from Bianchi et al. (2018), in which the random sample covers the full survey volume.

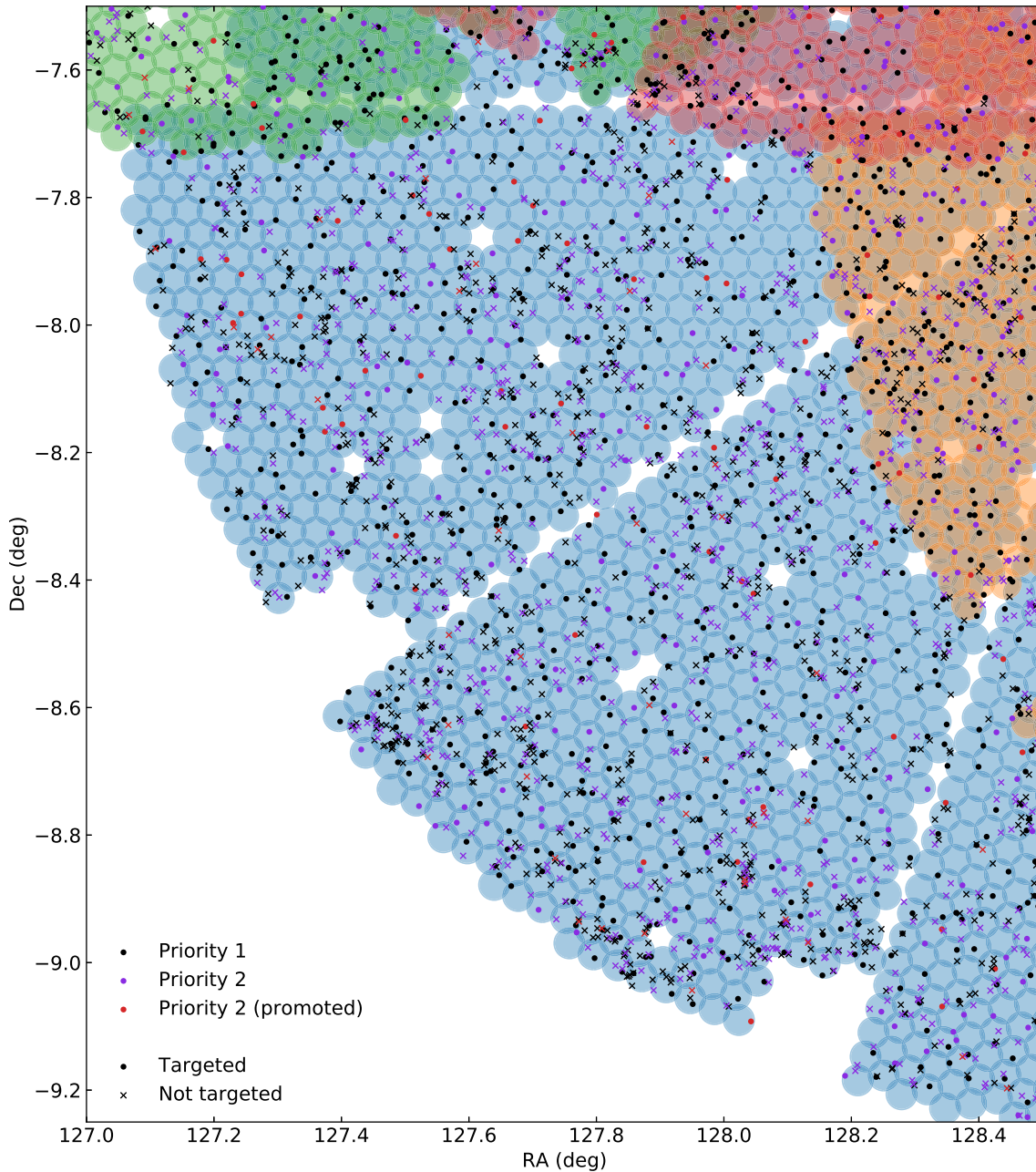


**Figure 3.** A zoom-in on a small section around the edge of the survey footprint of one survey simulation, showing the positions of BGS galaxies relative to fibre patrol regions. This survey simulation has zero dither, but 10 per cent of priority 2 galaxies are randomly promoted. Shaded circles indicate the patrol region of each fibre, with each neighbouring tile in a different colour. White regions cannot be reached by a fibre. Points indicate galaxies that are successfully assigned a fibre, while crosses show untargeted galaxies. The bright priority 1 sample is shown in black, and the faint priority 2 sample is in purple. Promoted priority 2 galaxies are shown in red.

We only consider targeting incompleteness caused by the fibre assignment algorithm. Redshift incompleteness due to redshift measurement failures and the effects of weather are left for future work.

### 3 FIBRE ASSIGNMENT COMPLETENESS

For a small region of sky, Fig. 3 shows the positions of targeted and untargeted galaxies in the BGS mock with the fibre patrol regions superimposed. This region is at the edge of the survey and is mostly covered by a single tile, shown in blue, with neighbouring tiles in

different colours. On the scale of the fibre patrol regions, the surface density of galaxies varies greatly. Some fibres have zero galaxies in their patrol region, leaving them free to target Milky Way stars, while fibres in dense regions can have 10 or more galaxies within their patrol region. It is clear to see that in dense regions, the fibre assignment completeness will be low, since only one galaxy can be assigned a fibre out of many potential targets. More galaxies can be targeted if there are multiple tile overlaps, which will make the completeness higher. In low-density regions, the completeness will be very high, since if there is only 1 galaxy within a fibre patrol region, the fibre will always be placed on that galaxy.

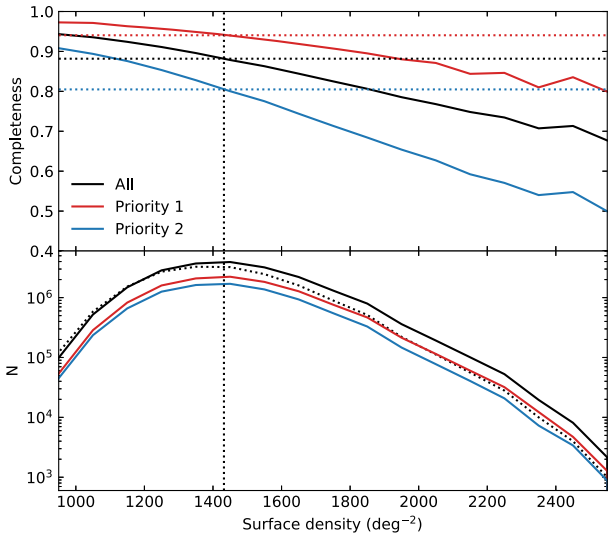


**Figure 4.** *Top panel:* Average fibre assignment completeness as a function of the surface density of all BGS galaxies, in HEALPIX pixels of area  $0.84 \text{ deg}^2$  ( $N_{\text{side}} = 64$ ) for all galaxies (black), priority 1 (red) and priority 2 (blue), after three passes with 10 per cent of priority 2 galaxies promoted. The vertical dotted line indicates the average surface density of the survey ( $1436 \text{ deg}^{-2}$ ), and horizontal dotted lines indicate the median completeness for the three samples (88 per cent, 94 per cent, and 80 per cent for all, priority 1 and priority 2 galaxies, respectively). *Bottom panel:* Histogram of the total number of objects in bins of surface density. The dotted black curve shows the number of HEALPIX pixels, scaled up by a factor of 1000.

The completeness due to surface density is quantified in Fig. 4. The upper panel shows the average completeness as a function of surface density, after three passes, in HEALPIX pixels (Górski et al. 2005) with area  $0.84 \text{ deg}^2$  ( $N_{\text{side}} = 64$ ), separately for all galaxies, and for priority 1 and 2 galaxies. The completeness decreases monotonically as the surface density of galaxies increases. Also, since priority 1 galaxies are preferentially targeted, they have a higher completeness than the priority 2 galaxies. The vertical dotted line indicates a surface density of  $1436 \text{ deg}^2$ , which is the average surface density of all (priority 1 and 2) galaxies, and horizontal dotted lines show the median completeness in HEALPIX pixels, which is 88 per cent, 94 per cent and 80 per cent for all, priority 1, and priority 2 galaxies respectively. The lower panel shows a histogram of the total number of galaxies, which peaks close to the average surface density. The black dotted curve shows the histogram of the densities of individual HEALPIX pixels, scaled up by a factor of 1000. The unscaled black dotted curve, multiplied by the average number of galaxies per pixel, produces the black solid curve. The variance in the surface density of pixels depends on the resolution. For pixels with area  $13.4 \text{ deg}^2$  ( $N_{\text{side}} = 16$ ), which is larger than the area of each tile, the surface density varies from the mean by a few hundred objects per square degree.

The fibre assignment completeness of galaxies in the BGS is driven by the surface density of galaxies, since it is not possible to place a fibre on every galaxy if the density of galaxies is greater than the density of fibres.<sup>8</sup> With multiple passes, the same area of sky will be re-observed several times, enabling some of these previously missed galaxies to be targeted. After the full three passes of the BGS, most of the footprint ( $\sim 80$  per cent) will have been covered by three

<sup>8</sup>Each tile of 5000 fibres has a radius of 1.605 deg, which corresponds to a fibre surface density of  $\sim 600 \text{ deg}^{-2}$ .

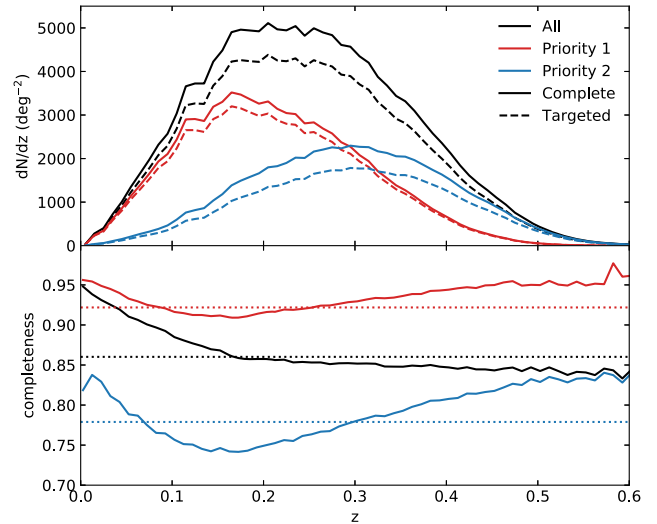


**Figure 5.** *Top panel:* Redshift distribution of galaxies before and after fibre assignment (solid and dashed curves), with the full three passes of tiles. The complete sample of BGS galaxies is shown in black, while priority 1 and priority 2 galaxies are in red and blue, respectively. *Bottom panel:* Completeness as a function of redshift for all, priority 1 and priority 2 galaxies. Horizontal dotted lines indicate the mean completeness (86 per cent, 92 per cent, and 78 per cent for all, priority 1 and priority 2 galaxies, respectively).

or four tiles (see Table 1), but the targeted catalogue will still be incomplete in high-density regions.

The upper panel of Fig. 5 shows the redshift distribution of galaxies in the BGS, before and after fibre assignment (solid and dashed curves). The lower panel shows the targeting completeness as a function of redshift, where the horizontal dotted lines indicate the average completeness. For the priority 1 and the priority 2 galaxies, this curve is non-monotonic. This is because haloes at high redshifts contain few galaxies brighter than the magnitude limit. These galaxies will not greatly enhance the surface density, and the completeness is high. At intermediate redshifts, many more galaxies per halo can be detected in haloes of the same mass, which will result in a much greater enhancement of the surface density, and therefore a lower completeness. At low redshifts, haloes of the same mass will contain an even greater number of galaxies brighter than the magnitude limit, but since they are nearby, they subtend a relatively large angle on the sky, and the perturbation to the surface density is low again. For the complete galaxy sample, the completeness is relatively flat at high redshifts, since the fraction of priority 2 galaxies increases with redshift.

The mean completeness (which differs slightly from the median completeness shown in Fig. 4) is  $\sim 86$  per cent, while for priority 1 and 2 galaxies it is  $\sim 92$  per cent and  $\sim 78$  per cent, respectively. These figures are for the case where 10 per cent of the priority 2 galaxies are given the same priority as the priority 1 galaxies. If there was no promotion of priority 2 objects, the priority 1 galaxies would be more complete ( $\sim 93$  per cent), but at the expense of the low-priority galaxies (see Table 3).

Fig. 6 shows the completeness of galaxies in haloes, as a function of the distance from the centre of their host halo, for haloes in different mass bins around the peak of the redshift distribution ( $0.15 < z < 0.25$ ). The panels, from top to bottom, show the completeness for haloes with masses  $M_{200\text{mean}} \sim 10^{15} h^{-1} \text{ Mpc}$ ,  $M_{200\text{mean}} \sim 10^{14} h^{-1} \text{ Mpc}$ ,  $M_{200\text{mean}} \sim$

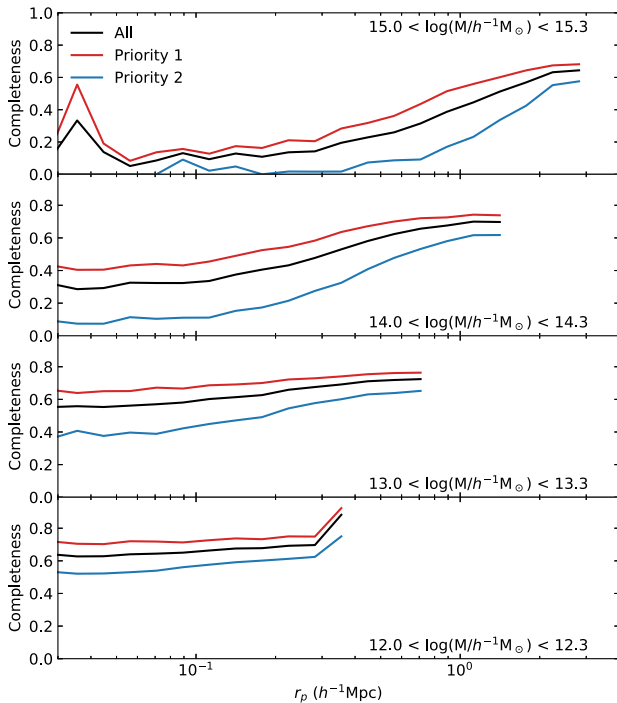


**Figure 6.** Targeting completeness of galaxies in haloes as a function of the transverse distance from the centre of their respective halo, for haloes in the redshift range  $0.15 < z < 0.25$ , after three passes. The completeness for all galaxies is shown in black, and for priority 1 and 2 galaxies in red and blue, respectively.

$10^{13} h^{-1} \text{Mpc}$ , and  $M_{200\text{mean}} \sim 10^{12} h^{-1} \text{Mpc}$ , respectively, plotted to the virial radius ( $R_{200\text{mean}}$ ).  $M_{200\text{mean}}$  is defined as the mass enclosed by a sphere of radius  $R_{200\text{mean}}$ , in which the average density is 200 times the mean density of the Universe. Close to the centre of large haloes, the surface density of galaxies is very high, and therefore, the completeness is very low. For  $10^{12} h^{-1} \text{Mpc}$  haloes, the average completeness near the centre is  $\sim 60$  per cent, but for the most massive haloes, this completeness is much lower. The spike close to the centre of  $M \sim 10^{15} h^{-1} \text{Mpc}$  haloes is due to noise. When measuring two-point clustering statistics, as we show in Section 4.3, the effect of this incompleteness can be corrected, and this is unbiased so long as each galaxy pair has a non-zero probability of being targeted. Since the completeness in clusters is low, care must be taken, for example, identifying clusters and voids and estimating velocity dispersions. The incompleteness must also be taken into account when estimating higher-point statistics. Our realizations of the fibre assignment algorithm could be used to develop correction procedures for these statistics.

The total number of objects targeted, and the completeness after each pass, is shown in Table 2 for all galaxies, priority 1 and 2 galaxies, and the subset of priority 2 galaxies that are promoted to the same priority as priority 1. Since faint galaxies are less clustered than bright galaxies, the promoted priority 2 galaxies have a higher completeness than the priority 1 galaxies. Most of the promoted galaxies are targeted in the first pass.

Table 3 shows how the final completeness after three passes is affected by the fraction of objects in the faint sub-sample promoted to high priority. The priority 1 sample is most complete with zero promotion (92.9 per cent), but the priority 2 sample is least complete (77 per cent), and certain priority 2 objects will always be missed due to conflicts with high-priority objects. As the fraction of priority

**Table 2.** Table showing the cumulative number of objects targeted after each pass, in millions, and the completeness, as a percentage. Priority 1 and priority 2 are the intrinsic priorities based on magnitude. Priority 2 (p) is the subset of priority 2 galaxies that are promoted to have the same priority as the bright priority 1 galaxies. The final row shows the cumulative number of unused fibres that are available to target Milky Way stars (in millions) after each pass, and the percentage of fibres that are unused after each pass. A total of  $\sim 9$  million fibres are available per pass, excluding standard stars and sky fibres (2000 pointings, each with 4500 available fibres).

Sample	Pass 1		Pass 2		Pass 3	
	$N_{\text{gal}}$	Per cent	$N_{\text{gal}}$	Per cent	$N_{\text{gal}}$	Per cent
All	7.54	35.6	13.78	65.0	18.24	86.0
Priority 1	5.15	42.7	8.84	73.3	11.11	92.2
Priority 2	2.39	26.1	4.95	54.1	7.12	77.8
Priority 2 (p)	0.79	86.2	0.84	92.4	0.85	93.2
Free fibres	1.49	16.5	4.30	23.8	8.89	32.8

**Table 3.** Table showing the number of objects targeted after three passes, in millions, and the completeness, in survey simulations where the percentage of promoted priority 2 galaxies is varied from 0 per cent to 40 per cent. Priority 1 and 2 galaxies are the bright and faint sub-samples, and priority 2 (p) are the promoted subset of priority 2 galaxies.

Promotion Per cent	Priority 1		Priority 2		Priority 2 (p)	
	$N_{\text{gal}}$	Per cent	$N_{\text{gal}}$	Per cent	$N_{\text{gal}}$	Per cent
0	11.12	92.9	7.04	77.0	–	–
5	11.15	92.5	7.08	77.4	0.43	93.7
10	11.11	92.2	7.12	77.8	0.85	93.2
15	11.07	91.8	7.17	78.4	1.28	93.1
20	11.02	91.5	7.21	78.9	1.69	92.6
25	11.00	91.1	7.26	79.3	2.11	92.5
30	10.94	90.7	7.30	79.8	2.52	92.0
35	10.89	90.3	7.35	80.3	2.93	91.7
40	10.84	90.0	7.39	80.8	3.34	91.4

2 objects is increased, the percentages converge to the average completeness of  $\sim 86$  per cent.

## 4 CORRECTING TWO-POINT CLUSTERING MEASUREMENTS

### 4.1 Mitigation techniques

The two-point correlation function at separation  $\vec{s}$  can be estimated using the estimator of Landy & Szalay (1993),

$$\xi(\vec{s}) = \frac{DD(\vec{s}) - 2DR(\vec{s}) + RR(\vec{s})}{RR(\vec{s})}, \quad (2)$$

where DD, DR, and RR are the normalized data-data, data-random, and random-random pair counts. If galaxies in the data catalogue are missing, the resulting correlation function will be biased. Mitigation techniques attempt to recover the correlation function of the parent sample from the sample of galaxies that are targeted.

#### 4.1.1 Nearest object

We use two different nearest object corrections. In the first correction, missing galaxies are assigned the redshift of the nearest targeted object on the sky (the approach taken in the SDSS survey

analyses in e.g. Zehavi et al. 2005; Berlind et al. 2006; Zehavi et al. 2011). The catalogue of galaxies is then cut to the volume-limited sample using these redshifts. Some of the untargeted objects will be assigned a redshift close to the true value, and will be correctly identified as part of the volume-limited sample, but the sample will be contaminated by other galaxies that are assigned incorrect redshifts. We refer to this correction as ‘nearest redshift’.

In the second correction, each galaxy is first given a weight of 1, and the weight of a missing galaxy is added to the nearest targeted object on the sky (e.g. in BAO analysis in the BOSS survey, Anderson et al. 2012, 2014a,b). For example, a targeted galaxy with no nearby untargeted galaxies would have weight 1. If there was a close galaxy that was not targeted, the weight would be transferred to the targeted galaxy, which would now have a weight of 2. We hereafter refer to this correction as ‘nearest weight’. The nearest weight correction can be seen as an approximation of the pair weighting method of Section 4.1.3 (see Bianchi & Percival 2017).

#### 4.1.2 Angular upweighting

When estimating the correlation function, galaxy pairs are up-weighted by the factor

$$W(\theta) = \frac{1 + w^{(p)}(\theta)}{1 + w(\theta)}, \quad (3)$$

where  $w^{(p)}(\theta)$  is the angular correlation function of the complete, parent sample of galaxies, and  $w(\theta)$  is the incomplete, targeted sample (e.g. the 2dFGRS analysis of Hawkins et al. 2003). This angular weighting by construction recovers the angular correlation of the parent sample. This correction makes the assumption that the targeted and untargeted galaxies are statistically equivalent in each angular bin, which is not necessarily true, and therefore it may not provide an adequate correction to the redshift–space correlation function.

#### 4.1.3 Pair inverse probability weights

The pair inverse probability (PIP) weighting scheme (Bianchi & Percival 2017) upweights each galaxy pair by the pair weight  $w_{ij} = 1/p_{ij}$ , where  $p_{ij}$  is the probability that the pair will be targeted. This probability can be estimated by running the fibre assignment code  $N_{\text{real}}$  times, where  $N_{\text{real}}$  is of the order of 100s or 1000s. For galaxy  $i$ , a vector  $\vec{w}_i$  of length  $N_{\text{real}}$  is stored, which contains a 1 if the galaxy is assigned a fibre, and a 0 otherwise. This vector can conveniently be stored as the bits of an integer (or several integers). The pair weight for galaxies  $i$  and  $j$  can be written as the dot-product of these vectors, but can be efficiently calculated using bitwise operations,

$$w_{ij} = \frac{N_{\text{real}}}{\vec{w}_i \cdot \vec{w}_j} \equiv \frac{N_{\text{real}}}{\text{popcount}(\vec{w}_i \& \vec{w}_j)}, \quad (4)$$

where  $\&$  is the bitwise ‘and’ operator, and `popcount` is a bitwise operator which sums together the bits of an integer.

The corrected DD counts are calculated from summing the pair weights of galaxies in the separation bin  $\vec{s}$ ,

$$\text{DD}_w(\vec{s}) = \sum_{\vec{s}_i - \vec{s}_j \approx \vec{s}} w_{ij} \frac{\text{DD}^{(p)}(\theta_{ij})}{\text{DD}_w(\theta_{ij})}, \quad (5)$$

where  $\text{DD}^{(p)}(\theta_{ij})$  are the angular DD counts of the parent sample, and  $\text{DD}_w(\theta_{ij})$  are the angular DD counts of the targeted sample but

weighted by the pair weights  $w_{ij}$  (from equation 4), i.e.

$$\text{DD}_w(\theta) = \sum_{\Delta\theta_{ij} \approx \theta} w_{ij}. \quad (6)$$

A similar correction is also applied to the DR counts, but this can be done using individual galaxy weights (see Section 4.1.4),

$$\text{DR}_w(\vec{s}) = \sum_{\vec{s}_i - \vec{s}_j \approx \vec{s}} w_i \frac{\text{DR}^{(p)}(\theta_{ij})}{\text{DR}_w(\theta_{ij})}. \quad (7)$$

In the case where there are no untargetable pairs, the PIP estimator is unbiased<sup>9</sup> without the additional angular weighting factor in equations (5) and (7). In this case, the ensemble mean of the angular weighting factor is unity and its inclusion is to reduce the variance in the estimator (see Percival & Bianchi 2017). However, in the case where there are untargetable pairs, the PIP estimator without this factor is biased.<sup>10</sup> Including the angular weighting corrects this bias if, at any separation, the untargeted pairs are an unbiased sample of all the pairs of that separation. The accuracy of this assumption depends on the details of the targeting algorithm. Our results provide a direct test of this for the case of the DESI BGS.

Bianchi et al. (2018) apply the PIP weighting scheme to a DESI ELG mock catalogue, and are able to recover unbiased clustering measurements. However, they do not dither the tile positions, and rely entirely on the angular weighting term to recover the small scale clustering. They also only include ELGs in their catalogue, so do not consider objects with different priorities.

#### 4.1.4 Individual inverse probability weights

Each galaxy is given an individual weight, which is the inverse of the probability that the galaxy will be targeted,  $w_i = 1/p_i$ . This can be estimated from the same bitwise vectors used to estimate the pair probabilities,

$$w_i = \frac{N_{\text{real}}}{\text{popcount}(\vec{w}_i)}. \quad (8)$$

If galaxies are given individual weights, the weight given to a pair of galaxies is the product of these two weights,  $w_{ij} = w_i w_j$ . This pair weight does not take into account any correlation between galaxy pairs, and will not produce an adequate correction on small scales where pairs are highly correlated.

## 4.2 Clustering estimates

Correlation functions are calculated using the publicly available parallelized correlation function code TWOPCF,<sup>11</sup> which contains an efficient implementation of the PIP weighting scheme. The code can also efficiently calculate jackknife errors in a single loop over the galaxy pairs (Stothert 2018). To create the random catalogue, we uniformly generate random points on the sky, only keeping those that fall within the patrol region of a fibre, with no dither, so that the

<sup>9</sup>Pair weighting takes into account correlations between galaxies in a pair, and is unbiased if each pair has a non-zero probability of being targeted. E.g. if a pair is targeted  $n$  times in  $N_{\text{real}}$  fibre assignment realizations, its weight is  $N_{\text{real}}/n$ , and it is targeted in  $n/N_{\text{real}}$  realizations, therefore the average weight is 1.

<sup>10</sup>Note that since the pairs with zero probability never enter the pair counts, the expectation value of the estimator is the clustering of the non-zero probability pairs.

<sup>11</sup>[https://github.com/istothert/two\\_pcf](https://github.com/istothert/two_pcf)

**Table 4.** Definition of the main and extended volume-limited samples. Both samples use the magnitude range  $-22 < M_r - 5 \log h < -21$ , where the absolute magnitudes are in the DECam  $r$ -band, and  $k$ -corrected to  $z = 0.1$ .  $z_{\min}$  and  $z_{\max}$  are the minimum and maximum redshifts,  $N_{\text{gal}}$  is the total number of galaxies in the sample,  $f_{\text{P1}}$  is the fraction of priority 1 galaxies, and  $\bar{n}$  is the average number density.

Sample	$z_{\min}$	$z_{\max}$	$N_{\text{gal}}$	$f_{\text{P1}}$	$\bar{n}$ ( $h^3 \text{Mpc}^{-3}$ )
Main	0.09	0.30	1532 903	1.00	$1.74 \times 10^{-3}$
Extended	0.09	0.35	2655 707	0.94	$1.94 \times 10^{-3}$

random catalogue covers the same footprint as the input catalogue. For illustrative purposes to compare correlation function correction techniques, we assume the parent volume-limited sample is known, and assign each object in the random catalogue a redshift randomly sampled from this distribution. This ensures that the number density of objects in the random catalogue has the same evolution as the data catalogue. In the real survey, the parent sample is not known beforehand, but the redshift distribution can be determined by weighting the redshift distribution of the targeted sample by the individual galaxy weights. We have checked, and the scatter between fibre assignment realizations of the weighted  $n(z)$  is within 1 per cent. Note that in the case of a flux-limited catalogue, the parent sample is known, and this is not an issue.

We also normalize the correlation function using the total number of objects in the parent sample. Again, in the real survey, this is not known, and the normalization factor should be obtained from the pair weights. However, we find that the difference between the normalization factor obtained from the parent sample and from the pair weights is small (a factor of  $\lesssim 10^{-3}$ ).

### 4.3 Results

We run the fibre assignment algorithm (Section 2) 2048 times on the BGS mock in order to generate weight vectors for each galaxy. In each realization, a random set of 10 per cent of the priority 2 galaxies are promoted to priority 1, and the tile positions are randomly dithered by an angle three times the patrol radius ( $3R_{\text{patrol}} = 4.45$  arcmin). We apply corrections to the clustering measured from two volume-limited samples, defined in Table 4. The maximum redshift of the main sample is chosen such that the sample only contains priority 1 galaxies, while the maximum redshift is increased for the extended sample so that it also includes priority 2 galaxies. The number densities of the two samples differ slightly, due to evolution of the number density with redshift in the mock.

#### 4.3.1 Galaxy weights

The fraction of galaxies assigned a fibre at least once after  $N_{\text{real}}$  realizations of the fibre assignment algorithm is shown in Fig. 7 for priority 1 and 2 galaxies, with one and three passes. To achieve a completeness of 99.99 per cent for priority 1 galaxies with three passes, only 20 realizations are needed, while the same completeness for priority 2 galaxies requires around 180 realizations. With only a single pass of tiles, the number of realizations needed increases to 50 and 400 for priority 1 and 2 galaxies, respectively. There are  $\sim 10$  galaxies that are not assigned a fibre in any of the 2048 realizations. This number is so small that it will have a negligible effect when applying the pair weighting correction to clustering measurements. This number of realizations is sufficient to estimate accurate pair probabilities for the vast majority of

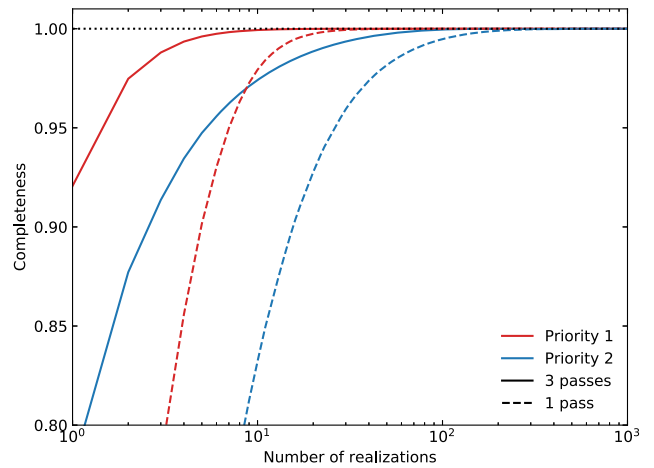


**Figure 7.** Completeness of galaxies that are assigned a fibre at least once after  $N$  random realizations of the fibre assignment algorithm. The full flux-limited priority 1 and priority 2 samples are shown in red and blue, respectively, where solid lines are with the full three passes of tiles, and dashed lines a single pass. In each realization, 10 per cent of priority 2 galaxies are randomly promoted to priority 1, and the tile centres are randomly dithered by three times the patrol radius.

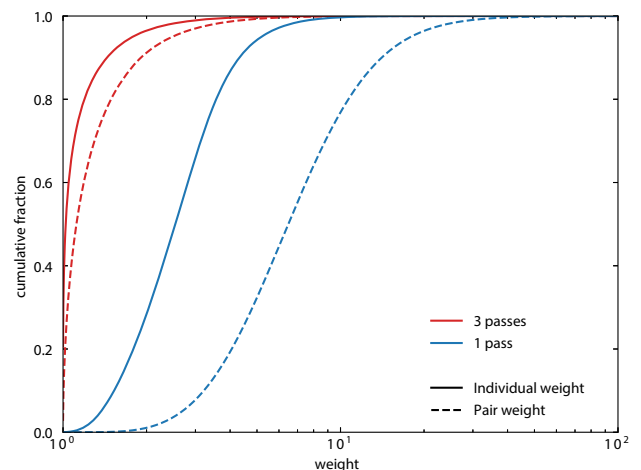


**Figure 8.** Cumulative distribution of individual galaxy weights (solid curves) and pair weights (dashed curves) of objects in the main volume-limited sample with 1 (blue) and 3 (red) passes of tiles. For the individual weights, the median, 90th and 99th percentiles are 1.03, 1.44, and 3.04, respectively, with three passes, and 2.54, 4.33, and 7.70 with a single pass. The same percentiles for the pair weights are 1.12, 1.91, and 4.39 (3 passes) and 6.50, 14.12, and 29.68 (one pass). After three passes, 16 per cent of objects are targeted in every realization, and have a weight exactly equal to 1, while 2.7 per cent of pairs are targeted in every realization.

galaxy pairs. However, note that the number of galaxies with zero probability, can only be used to infer a lower bound for the number of zero probability pairs.

The cumulative distribution of individual inverse probability (IIP) and PIP weights for the main volume-limited sample is shown in Fig. 8. Most of the priority 1 galaxies are targeted in every fibre assignment realization, and so the (non-cumulative) distribution of individual weights peaks at unity, with a tail extending to higher weights, due to objects in regions around the edge of the survey that are only covered by a single tile and have a low probability of being targeted. The pair weight distribution has a similar shape,

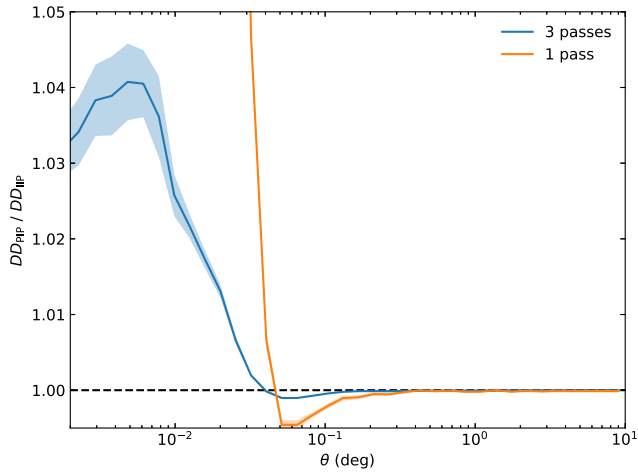


**Figure 9.** Ratio of angular DD counts calculated with pairwise, PIP, weights to that with individual IIP weights, for galaxies in the main volume-limited sample, after the full three passes of tiles (blue), and after 90 per cent of one pass (yellow). The solid curves are the average of 50 fibre assignment realizations, where the shaded regions indicate the  $1\sigma$  scatter. The black horizontal dashed line indicates a ratio of unity. The ratio on small scales after 1 pass is  $\sim 1.8$ .

but extends to higher weights. With only one pass, this distribution is very different, since  $\sim 90$  per cent of the survey is covered by a single tile. There are no objects targeted in every realization, and the individual weight distribution peaks at weight  $\sim 2$ , while the pair weight distribution peaks at  $\sim 5$ , with a tail extending out to very large weights.

Fig. 9 shows the ratio of the total DD counts in angular bins with PIP and IIP weights, for the main volume-limited sample, after one and three passes, illustrating how the correlation between pairs varies as a function of angular separation. On small scales, this ratio is greater than 1, indicating that the targeting probabilities are correlated, and  $w_{ij} > w_i w_j$ . At intermediate scales, there is a small negative correlation, which asymptotes towards 1 on large scales, where  $w_{ij} \sim w_i w_j$ . However, even at 10 deg, there is a very weak correlation, and the ratio is offset from 1 by  $\sim 10^{-5}$ . The size of the small-scale correlation depends on the galaxy sample and number of passes. After three passes, the DD counts differ by  $\sim 4$  per cent. After only single pass, since most of the area has single tile coverage, correlations are much larger, and the ratio of DD counts is  $\sim 1.8$ .

#### 4.3.2 Comparison of mitigation techniques

Fig. 10 compares the results of applying several commonly used correction methods to the monopole of the redshift space correlation function of the main volume-limited sample, after three passes. Each correction is applied to a single realization of the fibre assignment algorithm, and errors are estimated from 100 jackknife samples (see Fig. 1). The jackknife error is an estimate of the uncertainty in the clustering measurements due to the finite survey volume. The data are split into 100 regions of equal area, and the correlation function is calculated with each region omitted. The jackknife errors are taken from the square root of the diagonal terms of the covariance matrix. The ratio to the complete parent sample is shown in the lower panel. The purple curve shows the result of applying angular weighting, which by construction, reproduces the angular correlation function of the parent sample. However, this does not provide a satisfactory correction to the monopole. At scales of  $\sim 10 h^{-1}$  Mpc, it differs

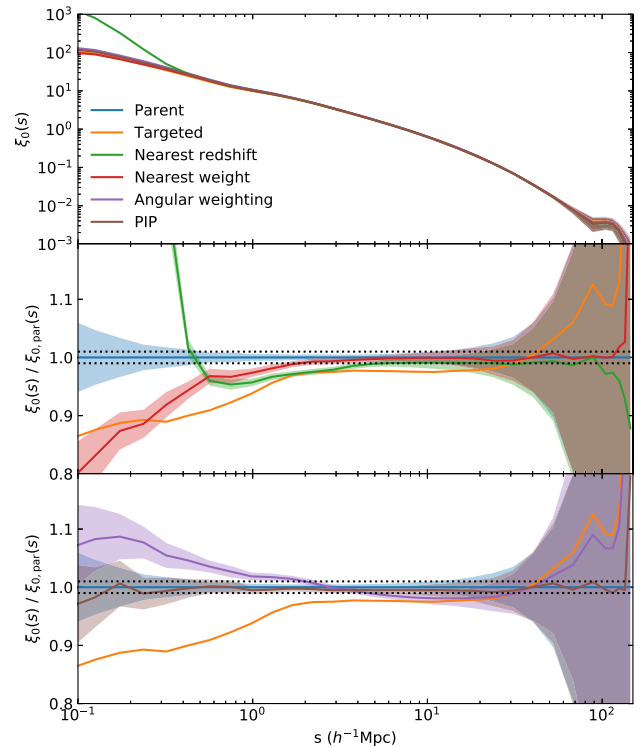


**Figure 10.** Monopole of the redshift space galaxy correlation function of the main volume-limited sample, with different corrections applied. The complete parent sample is shown in blue, targeted with no correction in yellow, assigning missing galaxies the redshift of the nearest targeted galaxy on the sky in green, transferring the weight of missing galaxies to the nearest targeted galaxy in red, angular upweighting in purple, and PIP weighting in brown. The ratio to the complete parent sample, for different correction methods, is split between the two lower panels for clarity. Shaded regions are errors estimated from 100 jackknife samples. Horizontal black dotted lines indicate  $\pm 1$  per cent. For  $s \gtrsim 20 h^{-1}$  Mpc, the scatter is almost the same for all methods.

from the parent sample by  $\sim 2$  per cent, which is approximately twice the statistical error in the complete sample. At small scales, close to  $0.1 h^{-1}$  Mpc, it differs by almost 10 per cent, while the statistical error in the parent sample is  $\sim 5$  per cent.

Assigning missing objects the redshift of the closest targeted object on the sky, shown by the green curve in Fig. 10, does better than angular weighting at large scales, correcting the monopole to a level of  $\sim 1$  per cent. However, this correction produces a strong artificial boost to the clustering at small scales. Some of the untargeted galaxies will be members of clusters, and if the nearest targeted object is also a member of the same cluster, the redshift it is assigned will be close to the true redshift. However, if two galaxies at different redshifts are close together on the sky by chance, the error in the assigned redshift could be large. This chance projection of galaxies boosts the redshift space monopole at  $0.1 h^{-1}$  Mpc by an order of magnitude.

Transferring the weight of missing galaxies to the nearest targeted galaxy on the sky, which is shown by the red curve in Fig. 10, produces a correction at large scales that is within 1 per cent. The total weight of galaxy clusters is correct, and so the large-scale clustering agrees with the parent sample. However, since small separation pairs are missing, the clustering on small scales is low.

The PIP correction, shown by the brown curve in Fig. 10, produces a correction within  $\sim 1$  per cent at all scales, even on small

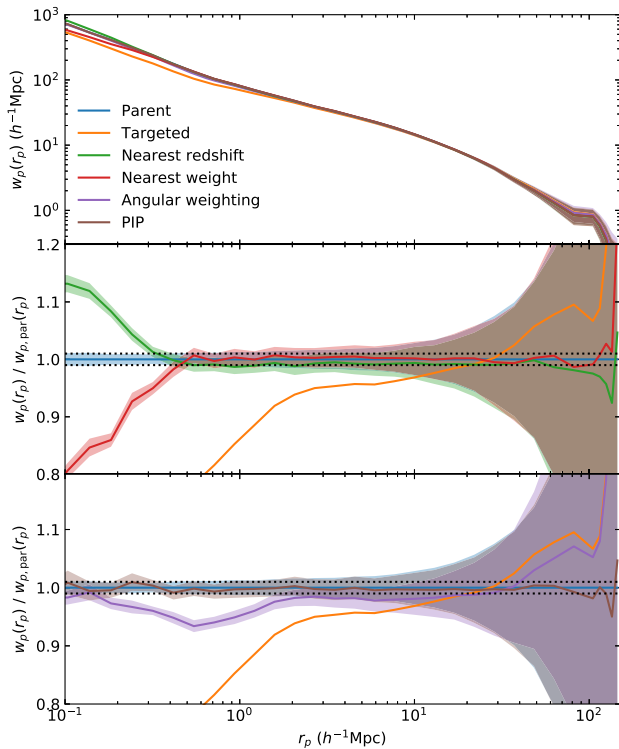


**Figure 11.** Projected correlation function of the main volume-limited sample, with the same corrections applied as Fig. 10. Shaded regions are errors estimated from 100 jackknife samples.

scales below a few  $h^{-1}$  Mpc where other correction methods fail. Here, the correction is only applied to a single fibre assignment realization, but in the next section, we apply the same correction to many realizations to check that is unbiased.

Note that only the monopole is shown in Fig. 10. We show in Section 4.3.4 the PIP scheme also works well for the quadrupole and hexadecapole. The other correction methods explored in this section fare less well for the higher order multipoles, only showing agreement with the parent sample on scales larger than a few 10s of  $h^{-1}$  Mpc.

The projected correlation function,

$$w_p(r_p) = 2 \int_0^{\pi_{\max}} \xi(r_p, \pi) d\pi, \quad (9)$$

is shown in Fig. 11, with the same corrections applied, and using  $\pi_{\max} = 120 h^{-1}$  Mpc. The two nearest redshift corrections are able to correct the projected correlation function to within 1 per cent down to a scale of  $\sim 0.5 h^{-1}$  Mpc. Since the projected correlation function integrates along the line of sight, it reduces the impact of galaxies that are assigned the wrong redshift. Again, the PIP weighting produces a correction to within  $\sim 1$  per cent on all scales.

Another correction method we have not considered here is to downweight objects in the random catalogue by the probability that a galaxy in that location could be targeted. However, this correction will only be unbiased if the completeness of galaxies is uncorrelated with density, which is not true in the BGS. The randoms would be downweighted in high-density regions, giving these regions less weight, and producing a biased estimate of the correlation function. Pinol et al. (2017) measure the power spectrum using weighted random catalogues, and show that it is unable to produce an adequate correction to the power spectrum, without removing low  $\mu$  bins.

### 4.3.3 Angular clustering with PIP weights

We now apply the PIP weighting to the angular correlation function. By construction, the angular correlation function of the parent sample is recovered exactly when the pair weighting and angular correction of equation (5) are both applied. However, it is interesting to see how well the PIP weighting on its own can recover the angular correlation function for a volume-limited sample, where in the real survey, the complete parent sample would not be known. To check that the correction is unbiased, we average the result of applying the correction to 50 fibre assignment realizations (which are a subset of the 2048 realizations used to estimate the pair weights). The result, after three passes, is shown in Fig. 12. The left-hand panels show the angular correlation function of the main volume-limited sample, with the ratio to the complete parent sample in the bottom panel. The parent sample is shown in blue, where the shaded region is the statistical error, estimated from 100 jackknife samples. The yellow curve shows the correlation function of galaxies assigned fibres in a single realization of fibre assignment, illustrating the size of the correction that needs to be made. The green curve illustrates the result of applying only the pair weighting, without the angular upweighting term, and is the mean of 50 realizations of fibre assignment. The shaded region indicates the  $1\sigma$  scatter between these realizations. This is the additional error due to measuring the clustering from a subset of the objects in the parent sample, and we aim for this to be small compared to the statistical error in the parent sample. On large scales, the pair weighting does an excellent job of correcting the angular clustering. The mean is unbiased, and the scatter is within 1 per cent for angular scales between  $\sim 0.03$  deg and 1 deg. This is much smaller than the statistical error in the parent sample, which is of the order of a few per cent, increasing on larger scales. However, on small scales, less than  $0.5R_{\text{patrol}}$ , there is a small bias of a few per cent. This bias is due to pairs of galaxies around the edge of the survey, in regions covered by only a single tile. Pairs of galaxies with a very small angular separation in these regions can never be targeted due to fibre collisions, even when the tiles are dithered. Since these pairs have a zero probability of being targeted, this results in a bias, which is corrected for by the angular upweighting term. It is not guaranteed that this angular correction will be accurate since, for example, missing pairs could occur preferentially in triplets, and therefore be statistically distinct from targeted pairs of the same separation. However, we find that this is not the case, and the missed pairs fall in the regions of single tile coverage. Alternatively, the edge of the survey could be trimmed, removing the regions covered by a single tile, which is only a small percentage of the footprint ( $\sim 3$  per cent, see Table 1). Another alternative strategy is discussed in Section 4.4.

For comparison, the purple curve shows the result of applying individual galaxy weights to the same set of realizations. At small scales, applying individual weights results in a larger bias than pair weights, and this bias extends to larger angular scales. This is because individual galaxy weights do not take into account any correlation between galaxy pairs. For example, if it is difficult to target both galaxies in a pair due to fibre collisions, but relatively easy to target one or the other individually, calculating the pair probability from individual probabilities is biased since  $p_i p_j > p_{ij}$ . On large scales, if there are no correlations between pairs,  $p_i p_j = p_{ij}$ , and using individual weights should produce the same result as pair weights. However, in Fig 12, there is still a small difference between the green and purple curves on large scales. Even at scales of  $\sim 10$  deg, there is still some correlation between galaxy pairs, although this is very small, with a fractional difference in the DD

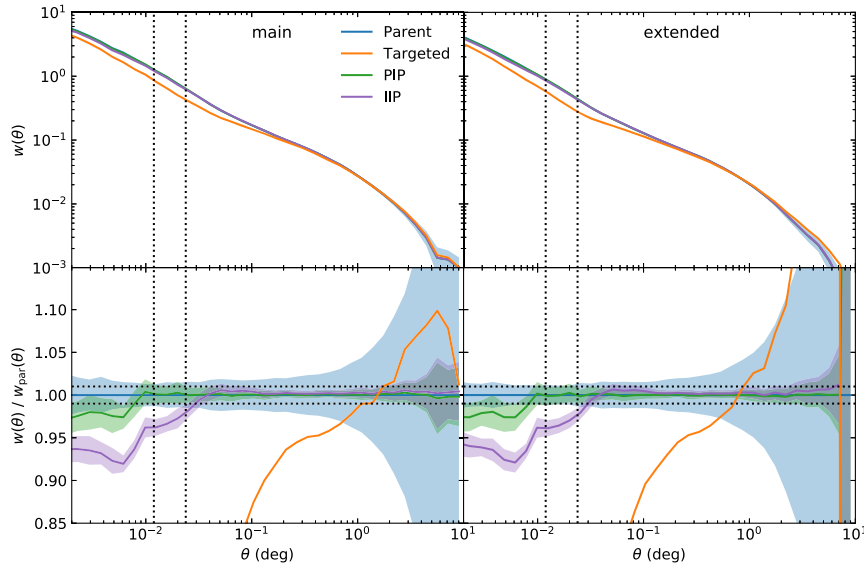


**Figure 12.** Angular correlation function for the main volume-limited sample that only contains priority 1 galaxies (left), and the extended volume-limited sample that also contains priority 2 galaxies (right), after the full three passes of tiles. The bottom panels show the ratio to the complete parent sample. The parent sample is shown in blue, where the shaded region indicates the error from 100 jackknife samples. The yellow curve illustrates the angular correlation function from one realization of fibre assignment, with no correction. Green and purple curves are the results of applying pair weighting and individual galaxy weighting, respectively, averaged over 50 realizations. The shaded regions indicate the scatter between these 50 realizations. Vertical dotted lines indicate the angular scale of  $R_{\text{patrol}}$  and  $0.5R_{\text{patrol}}$  and the horizontal lines indicate  $\pm 1$  per cent.

counts of  $\Delta\text{DD}/\text{DD} \sim 10^{-5}$ . The fractional error in  $\xi$  is given by

$$\frac{\Delta\xi}{\xi} \approx \frac{\Delta\text{DD}}{\text{DD}} \frac{(1 + \xi)}{\xi}. \quad (10)$$

On large scales,  $\xi \sim 10^{-3}$ , which results in a fractional difference of  $\Delta\xi/\xi \sim 1$  per cent, which is a small, but noticeable difference in the correlation function.

The right-hand panels of Fig. 12 shows the result of applying the same corrections to the extended volume-limited sample, which also contains priority 2 galaxies. By giving the priority 2 galaxies, a small probability of being promoted to priority 1, this gives every pair of priority 2 galaxies a non-zero probability of being targeted, and therefore applying the pair weighting correction produces an unbiased result on large scales. There is still a small bias on small scales for the same reason as in the main sample.

Fig. 13 shows the angular correlation function after only a single pass of tiles, with a random 10 per cent of the tiles missing, for the same volume-limited samples. With only one pass of tiles, the catalogue of fibre assigned galaxies is much less complete, and a larger correction is required.

Since most of the footprint is covered by a single tile ( $\sim 90$  per cent, see Table 1), the bias on scales less than  $0.5R_{\text{patrol}}$  is much larger than after three passes. Since there are overlaps between neighbouring tiles, the pair counts on these scales are low, but not zero. Pair weighting must be combined with angular upweighting in order to correct the clustering on these scales.

On larger scales, pair weights on their own are able to produce an unbiased correction, although the scatter between realizations is larger than with three passes, but on scales above 1 deg, this scatter is approximately half of the statistical error of the parent sample.

#### 4.3.4 Correlation function multipoles with PIP weights

The Legendre multipoles of the redshift space correlation function for the main sample after three passes are shown in Fig. 14. At large scales, the PIP weighting on its own is unbiased and does a good job of correcting the measured clustering. Between 1 and  $10 h^{-1}$  Mpc, the scatter between realizations in the monopole is well within 1 per cent, and even for the hexadecapole the scatter is around 1 per cent. Note that the scatter in the quadrupole and hexadecapole appears to be large at  $\sim 1 h^{-1}$  Mpc and  $\sim 5 h^{-1}$  Mpc, respectively, but this is just because the curves in the upper panels go through zero.

On small scales, similarly to what was seen in the angular correlation function, applying the PIP weighting on its own produces a biased result, due to pairs that cannot be targeted in regions covered by a single tile. Most of this area covered by a single tile is located around the edge of the footprint. We again find that including the angular weighting term corrects for this small bias.

Fig. 15 is the same, but for the extended sample. The results look similar to that of the main sample, showing that including priority 2 galaxies does not produce any biases.

Figs 16 and 17 show the results of applying the same corrections to the same volume-limited samples, but with only 90 per cent of one pass of tiles. Since the survey is much more incomplete, the correction that must be applied is larger. On large scales, applying the PIP weights on their own produces an unbiased correction, but with larger scatter between fibre assignment realizations compared to the three pass case. On small scales, the bias is much larger for PIP alone, but combining with angular weighting is able to correct this large small scale bias to within the errors.

After the full three passes of tiles, the scatter between realizations is much smaller than the statistical error in the parent sample on all scales. With only a single pass, this scatter is much larger, and on small scales becomes larger than the statistical error. The scatter is large after one pass because the sample is highly incomplete

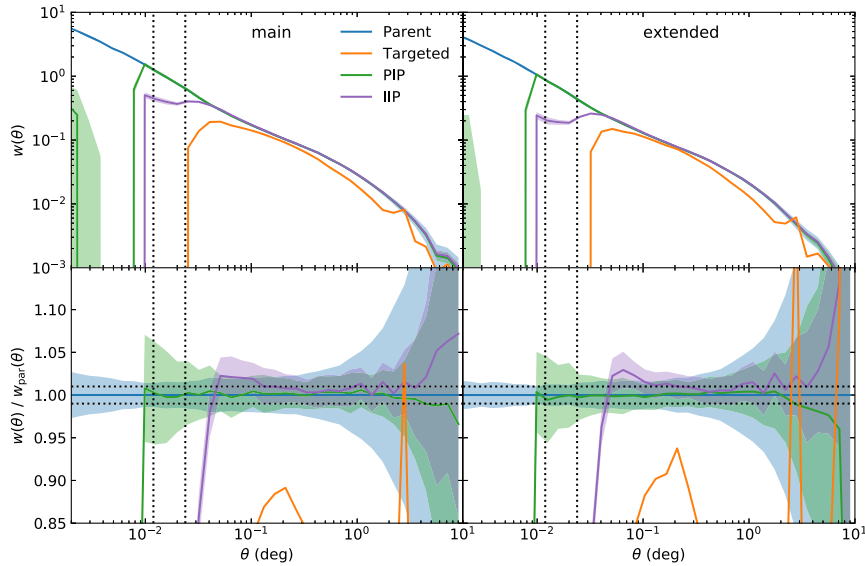


**Figure 13.** As Fig. 12 but after only one pass of tiles, and with 10 per cent of the tiles missing. This illustrates the data that might have been obtained after one-third of the complete survey, with a survey strategy that prioritized area over completeness.

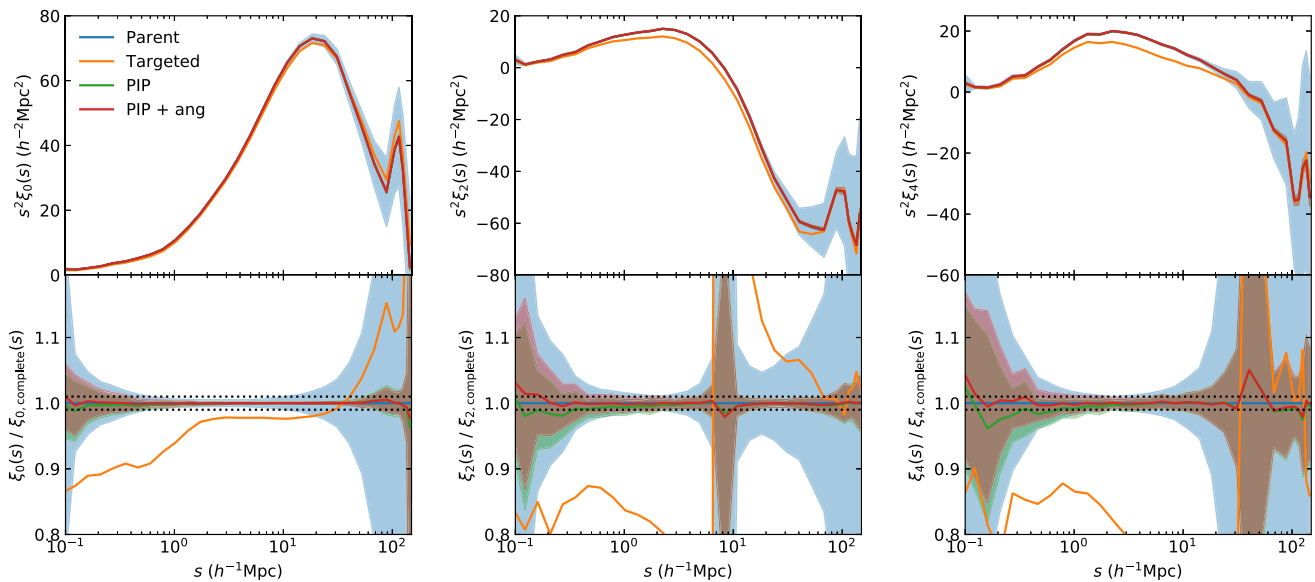


**Figure 14.** Monopole,  $\xi_0(s)$ , quadrupole,  $\xi_2(s)$ , and hexadecapole,  $\xi_4(s)$ , of the redshift space galaxy correlation function for the main volume-limited sample. The ratio to the complete parent sample is shown in the bottom panel. The parent sample is indicated by the blue curve, where the shaded blue region is the error from 100 jackknife samples. The green curve is the average of 50 realizations, corrected with only PIP weighting. The red curve is corrected using both PIP and angular weighting. Shaded green and red regions indicate  $1\sigma$ , estimated from the scatter between the 50 realizations.

(e.g. for the main volume-limited sample,  $\sim 38$  per cent of objects are assigned a fibre in each realization), and most objects have a large weight (the median weight is 2.54, see Fig. 8). After three passes, the scatter is much smaller, since the completeness of the main sample is much higher ( $\sim 82$  per cent), and most objects have a weight close to unity. 90 per cent of the one-pass survey area is covered by a single tile, and the completeness of close pairs is very low, due to fibre collisions. Each pair will also have a very large weight, which results in the very large scatter on small scales. The completeness of pairs on small scales is much higher with multiple passes, and therefore the scatter is much smaller.

While the average of many fibre assignment realizations is unbiased, the real survey is only a single realization, and after one pass it is likely that there will be a large scatter between the corrected clustering measurements and the true clustering at small scales. Multiple passes are therefore necessary in order to obtain precise clustering measurements on these scales. On large scales, the scatter is smaller than the statistical error after one pass, so it will be possible to make precise BAO and large-scale RSD measurements. However, the uncertainty in these measurements will be greatly reduced after the subsequent passes. Multiple passes will also reduce the incompleteness due to redshift measurement failures, as it will give these galaxies another chance to be targeted.

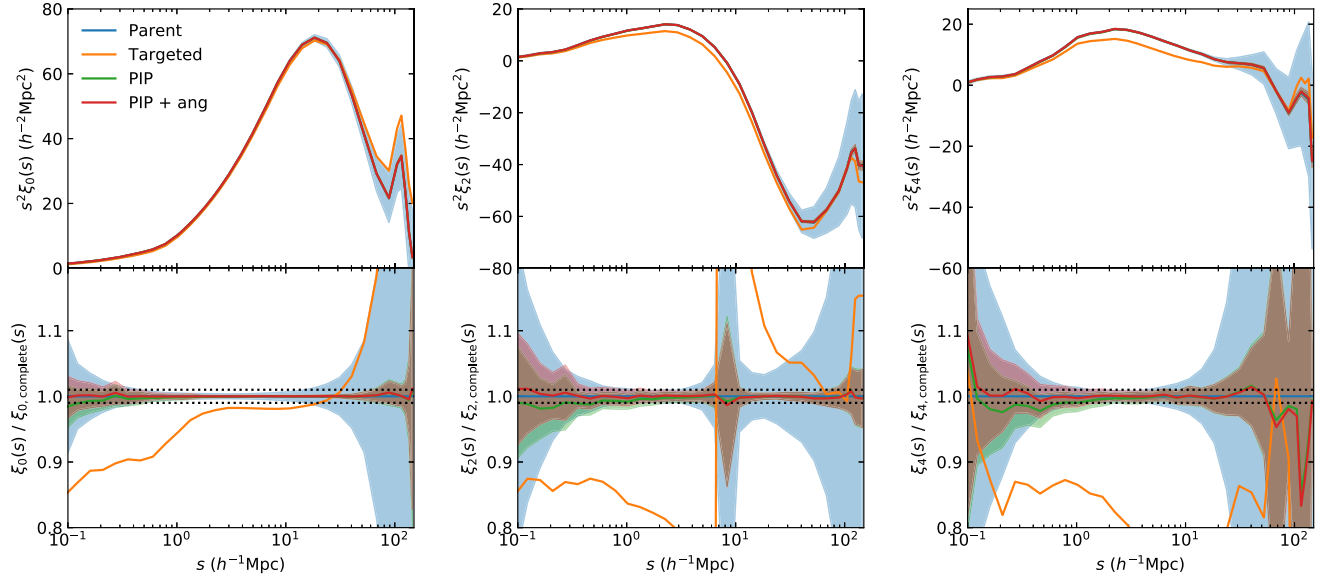


**Figure 15.** As Fig. 14, but for the extended volume-limited sample, which contains both priority 1 and 2 galaxies.

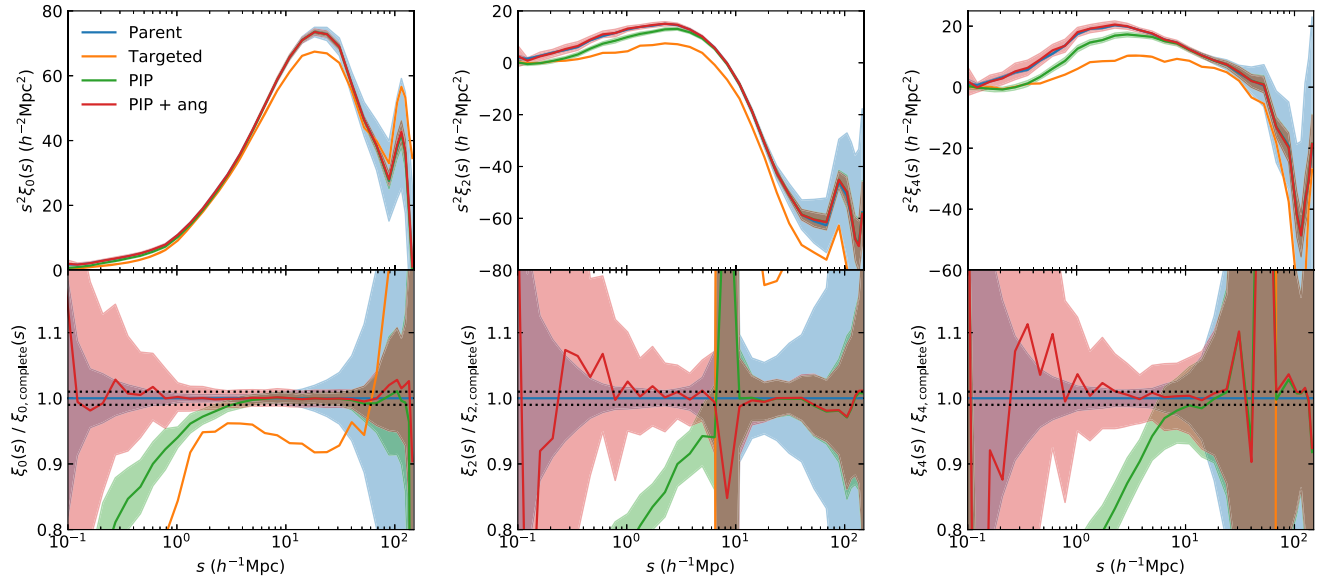


**Figure 16.** As Fig. 14, but for the case of only a single pass of tiles.

To make precise small-scale RSD measurements, a single pass is not sufficient.

The shot noise in these galaxy clustering measurements could potentially be reduced by capping the pair weights at some maximum value. Strictly speaking, the PIP weighting would no longer be unbiased, but this bias can be reduced by the angular weighting term, using these capped weights. We find that for the main sample after one pass, capping the weights at a maximum value of 100 (0.01 per cent of pairs) has a negligible effect on the monopole, but reduces the scatter in the quadrupole and hexadecapole at scales of  $\sim 1 h^{-1} \text{Mpc}$  by a few per cent. Capping the weight at 25 ( $\sim 2$  per cent of pairs) introduces systematics, which are not corrected for completely by the angular weighting. On large scales, there is a negligible change in the scatter, and the small bias that is introduced is within the errors. On small scales, this bias is larger, but is still within the large errors.

#### 4.4 Discussion

We have shown in the previous section that the PIP weighting scheme, in combination with angular upweighting, is able to produce an unbiased correction to clustering measurements in the BGS, even for a highly incomplete survey.

One simplifying assumption we have made is that the galaxies in the parent sample are known. The angular weighting term from equation (5) includes  $DD^{(p)}$ , the angular data–data pair counts of the complete parent sample (and similarly for the DR counts,  $DR^{(p)}$ ). For a flux-limited sample, the parent sample is known, but this is not true in the case of a volume-limited sample, since every redshift would need to be measured to determine an absolute magnitude, and hence which galaxies belong in the sample. When applying the angular weighting, we have used the true parent sample, which in the real survey would not be known.

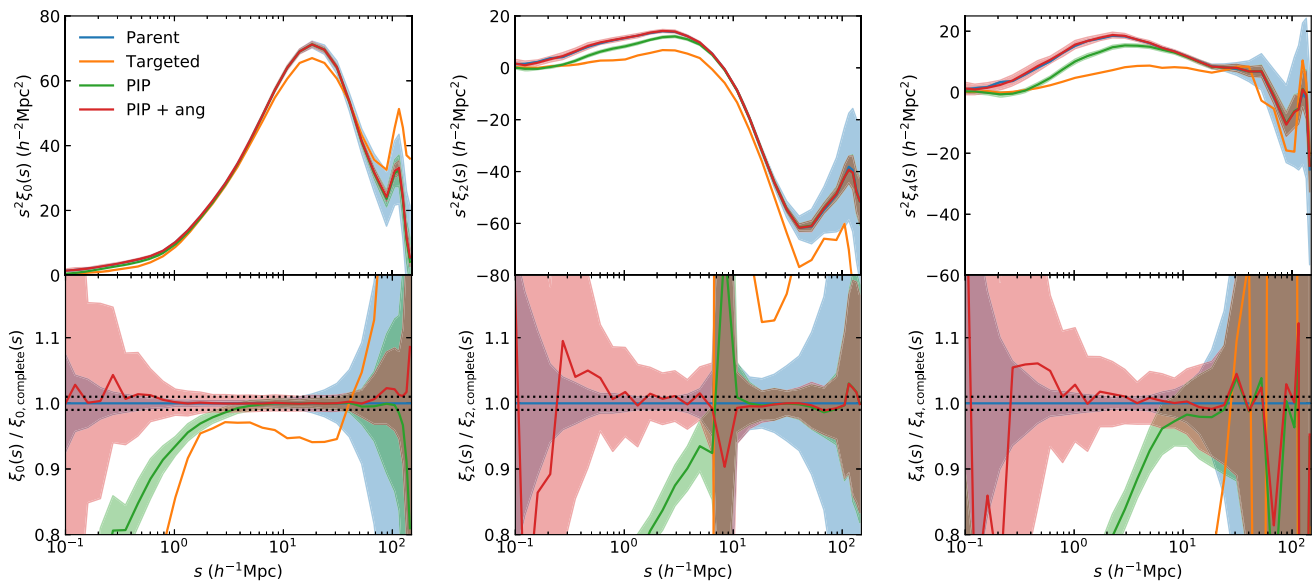


**Figure 17.** As Fig. 14, but for the extended volume-limited sample, after only a single pass of tiles.

In order to calculate pair weights, we dither the catalogue by a small angle in each realization of fibre assignment. For galaxies close to the edge of the survey, in half of the realizations they will fall outside the footprint, which results in these galaxies having larger weights than galaxies in the centre. In the actual survey, the dither is zero, which is a special case where no objects fall off the edge, and is not strictly represented in the ensemble of realizations. However, we find no measurable bias as only a very small fraction of objects are affected.

An issue that affects the real survey that we have not considered is stellar contamination. A small fraction of objects in the catalogue of potential targets are stars that have been misclassified as galaxies. If a fibre is placed on one of these objects, and a spectrum measured, it can be determined that it is a star and not a galaxy. Since the PIP weighting scheme can produce an unbiased correction to clustering measurements of any sub-sample of galaxies, the misclassified stars can simply be removed when estimating the correlation function. As long as the stars are included when running the fibre assignment algorithm many times to estimate the PIP weights, this will produce unbiased clustering measurements.

An alternative way to dither the catalogue would be to place the survey tiling randomly on the full sky, with a random orientation. This has the advantage that the undithered catalogue is not a special case, and could be drawn from these random tile positions. Also, every part of the sky has a non-zero probability of being in an area of the survey covered by multiple tile overlaps, giving every pair, even at very small separations, a non-zero probability of being targeted. This means that  $w_{ij}$  pair weights without angular weighting can produce an unbiased correction, so the correction can be applied without knowledge of the complete parent sample. However, in many of these fibre assignment realizations, the tiling would cover large areas of the sky which are outside the BGS footprint. Despite this, we expect that the total number of realizations needed to accurately estimate pair weights will be smaller, since the tail of pairs with extremely high weights are much more likely to be targeted in the realizations where they are covered by multiple tile overlaps.

A similar method to this is used in Mohammad et al. (2018), where in order to estimate pair weights for galaxies in the VIPERS

survey, the parent catalogue is rotated by angles of 0, 90, 180, and 270 deg, and the spectroscopic mask is moved spatially. The PIP weighting scheme is shown to work well, and this is the only published example of applying the PIP weights to a real dataset.

With large dithers across the full sky, it is also necessary to modify the definition of pair weights to take into account that galaxies will fall outside the survey tiling in many of these realizations of fibre assignment. Consider a perfect survey in which if two galaxies fall within the survey tiling, it is always possible to target the pair, so all pairs should have the same weight. If the pair have a very small angular separation, then in one-third of realizations they will fall within the tiling and be able to be targeted, so they would have a pair weight of 3, using equation (4). However, if a pair has a very large separation, it can be unlikely that both fall within the tiling at the same time in a random realization, so the pair probability is low and therefore the weight will be much larger than 3. Equation (4) incorrectly gives pairs of different separations different weights. Instead, the pair weight can be redefined as

$$w_{ij} = \frac{\vec{c}_i \cdot \vec{c}_j}{\vec{w}_i \cdot \vec{w}_j}, \quad (11)$$

where  $\vec{c}_i$  is a bitwise coverage vector that contains a 1 if it is possible to place a fibre on galaxy  $i$  (i.e. the galaxy lies within the patrol region of a fibre though it may happen not to be targeted) in that realization, and 0 otherwise.<sup>12</sup> Applying this definition in the above example results in all pairs having a weight of 1, as expected.

We have only shown the results of applying the correction to volume-limited samples with a number density  $\sim 2 \times 10^{-3} h^3 \text{ Mpc}^{-3}$ . We have also applied the correction to volume-limited samples of different number densities, and samples defined by a colour cut, and we find that applying the PIP correction with angular weighting will produce an unbiased correction.

<sup>12</sup>The ability to use bitwise coverage vectors is implemented in the correlation function code TWOPCF (Stothert 2018).

## 5 CONCLUSIONS

The DESI BGS will be a highly complete, flux-limited spectroscopic survey of low-redshift galaxies, an order of magnitude larger than existing galaxy catalogues, with the primary science aims of BAO and RSD analysis. Fibres in the focal plane of the telescope are controlled by robotic fibre positioners, each of which can place a fibre on any galaxy within a small patrol region, leading to incompleteness in the catalogue due to fibre collisions, and the fixed density of fibres over large regions in each tile. This leaves a non-trivial impact on clustering measurements, and it is essential that these biases can be corrected.

We have quantified the targeting completeness in the BGS by applying the DESI fibre assignment algorithm to a BGS mock catalogue. To ensure each galaxy has a non-zero probability of being targeted, and to maximize the number of pairs that can be targeted, we randomly promote 10 per cent of faint priority galaxies to the same priority as the bright priority 1 galaxies, and dither the tile positions by a small angle of three times the fibre patrol radius.

The main determinant of completeness in the BGS is the surface density of galaxies. Completeness is high in low surface density regions (e.g. over 95 per cent for priority 1 galaxies after three passes), but drops significantly in the most overdense regions. Close to the centre of the very most massive haloes ( $\sim 10^{15} h^{-1} M_{\odot}$ ), the completeness can be as low as 10 per cent or less.

We applied several correlation function correction methods to volume-limited samples from the BGS mock catalogue, where the incompleteness is due to fibre assignment only. This is done for a highly complete survey with three passes of tiles, and a highly incomplete survey, with one pass and 10 per cent of the tiles missing. Using standard angular upweighting, or assigning missing galaxies the redshift of the nearest targeted galaxy provide an unsatisfactory correction to the correlation function monopole on small scales below a few Mpc (and a few 10s of Mpc for the higher order multipoles).

After three passes of tiles, the method of Bianchi & Percival (2017), which combines galaxy pair weights with an angular weighting, is able to produce an unbiased correction to the angular and redshift space correlation functions, where the scatter between fibre assignment realizations is much smaller than the statistical error in the complete parent sample. The angular weighting term is required to correct a small bias on small scales caused by untargetable pairs around the edge of the survey footprint. After one pass, the correction is again unbiased, but the scatter between realizations is much larger, and on small scales the method relies heavily on angular weighting. More than one pass will be needed to make precise RSD measurements on small scales.

We propose an alternative method to dither the tiles, where the entire survey tiling is positioned randomly on the full sky, and the pair weight definition takes into account realizations in which objects cannot be targeted. This has the advantage that pair weighting on its own can produce an unbiased correction without relying on angular weighting.

## ACKNOWLEDGEMENTS

This work was supported by the Science and Technology Facilities Council (ST/M503472/1). AS, JH, SC, LS, PN, and CB

acknowledge the support of the Science and Technology Facilities Council (ST/L00075X/1). JH is supported by the European Research Council (ERC-StG-716532-PUNCA) and the Durham Research Council (ERC-StG-716532-PUNCA) and the Durham co-fund Junior Research Fellowship. LS acknowledges the support of the Science and Technology Facilities Council (ST/J501013/1). PN acknowledges the support of the Royal Society through the award of a University Research Fellowship. JEFR acknowledges support from COLCIENCIAS Contract No. 287-2016, Project 1204-712-50459.

This work used the DiRAC Data Centric system at Durham University, operated by the Institute for Computational Cosmology on behalf of the STFC DiRAC HPC Facility ([www.dirac.ac.uk](http://www.dirac.ac.uk)). This equipment was funded by BIS National E-infrastructure capital grant ST/K00042X/1, STFC capital grants ST/H008519/1 and ST/K00087X/1, STFC DiRAC Operations grant ST/K003267/1 and Durham University. DiRAC is part of the National E-Infrastructure.

## REFERENCES

- Abazajian K. N. et al., 2009, *ApJS*, 182, 543  
 Anderson L. et al., 2012, *MNRAS*, 427, 3435  
 Anderson L. et al., 2014a, *MNRAS*, 439, 83  
 Anderson L. et al., 2014b, *MNRAS*, 441, 24  
 Berlind A. A. et al., 2006, *ApJS*, 167, 1  
 Bianchi D. et al., 2018, *MNRAS*, 481, 2338  
 Bianchi D., Percival W. J., 2017, *MNRAS*, 472, 1106  
 Blanton M. R. et al., 2003, *ApJ*, 592, 819  
 Burden A., Padmanabhan N., Cahn R. N., White M. J., Samushia L., 2017, *J. Cosmol. Astropart. Phys.*, 3, 001  
 DESI Collaboration et al., 2016a, preprint ([arXiv:1611.00036](https://arxiv.org/abs/1611.00036))  
 DESI Collaboration et al., 2016b, preprint ([arXiv:1611.00037](https://arxiv.org/abs/1611.00037))  
 Farrow D. J. et al., 2015, *MNRAS*, 454, 2120  
 Górski K. M., Hivon E., Banday A. J., Wandelt B. D., Hansen F. K., Reinecke M., Bartelmann M., 2005, *ApJ*, 622, 759  
 Guo H., Zehavi I., Zheng Z., 2012, *ApJ*, 756, 127  
 Guzzo L. et al., 2008, *Nature*, 451, 541  
 Hawkins E. et al., 2003, *MNRAS*, 346, 78  
 Landy S. D., Szalay A. S., 1993, *ApJ*, 412, 64  
 Loveday J. et al., 2012, *MNRAS*, 420, 1239  
 Mohammad F. G. et al., 2018, *A&A*, 619, A17  
 Percival W. J., Bianchi D., 2017, *MNRAS*, 472, L40  
 Pinol L., Cahn R. N., Hand N., Seljak U., White M., 2017, *J. Cosmol. Astropart. Phys.*, 4, 008  
 Planck Collaboration VI, 2018, preprint ([arXiv:1807.06209](https://arxiv.org/abs/1807.06209))  
 Robotham A. et al., 2010, *PASA*, 27, 76  
 Schubnell M. et al., 2016, *Proc. SPIE*, 9908, 990892  
 Seo H.-J., Eisenstein D. J., 2003, *ApJ*, 598, 720  
 Smith A., Cole S., Baugh C., Zheng Z., Angulo R., Norberg P., Zehavi I., 2017, *MNRAS*, 470, 4646  
 Spergel D. N. et al., 2003, *ApJS*, 148, 175  
 Stothert L., 2018, PhD thesis, University of Durham  
 Strauss M. A. et al., 2002, *AJ*, 124, 1810  
 Zehavi I. et al., 2005, *ApJ*, 630, 1  
 Zehavi I. et al., 2011, *ApJ*, 736, 59

This paper has been typeset from a  $\text{\LaTeX}$  file prepared by the author.